Stability and Bifurcation of Fluid Flow Model of TCP Network versus Time Delay

Xiaolu Yan, Tiaoyang Cai, and Ranran Zhang

***Abstract*—In this paper, we consider the nonlinear dynamics of the fluid model of transmission control protocol (TCP) network, including the local stability and the Hopf bifurcation. We specify the time delay stabilization range of the system at equilibrium and propose an effective method to determine the direction and stability of the bifurcation producing periodic solutions. In the linear analysis process, the τ-decomposition technique is utilized to deal with the local stability problem of the time delay system, and an explicit expression for the time delay stability region is provided. For the nonlinear analysis part, the formulas for determining the direction of Hopf bifurcation and the stability of the periodic solution are derived with the help of the central manifold theorem and the canonical type theory as the basis, which enable the bifurcation parameters to be calculated directly. Finally, the accuracy and practicality of the theoretical analysis in this paper are verified through a series of typical numerical simulation cases.**

***Index Terms*—Transmission control protocol (TCP), Hopf bifurcation, stability, congestion control**

I. Introduction

In recent years, network congestion [1, 2] has become a serious and challenging problem. Network congestion occurs when user traffic demand on the network exceeds its carrying capacity and processing limit. This phenomenon has received much attention within the field of network science. Network congestion not only increases the packet loss rate and end-to-end delay but, in severe cases, it can also lead to the paralysis of the entire system [3–6]. In the face of a large number of users and high information flow, how to guarantee the efficient transmission of information and maintain the stability of network communication has become a common concern.

A series of control algorithms for various network characteristics have been proposed. Shen et al. analyzed fluid flow based transmission control protocol (TCP) and active queue management (AQM) network system model [7]. They proposed a fixed time adaptive congestion control algorithm for a nonlinear network system model with unknown user datagram protocol (UDP) traffic and unmodeled uncertainty. In Ref. [8], Ghosh et al. studied the composite transmission control protocol across three different topologies. They focused on TCP with a small drop tail buffer and emphasized the local stability and Hopf bifurcation of the system. Jin et al. studied the nonlinear dynamics, including local stability and periodic solutions of TCP/AQM networks [9]. Yu et al. considered the Hopf bifurcation control problem in the second-order Westwood+ TCP flow control model [10]. A dynamic time delay state feedback controller was proposed to delay the occurrence of Hopf bifurcation. In Ref. [11], Cai et al. studied a class of fast transmission control protocol networks with delayed state feedback mechanisms in terms of nonlinear dynamics, including local stability and periodic bifurcation. Manjunath and Raina investigated composite TCP queue management [12] with a proportional-integral strategy on internet routers, considered a nonlinear fluid model for composite TCP systems, and derived sufficient conditions for local stability. In Ref. [13], Vardoyan et al. proposed a generic modeling scheme consisting of a set of delay types (retarded functional differential equation, RFDE) and a congestion window as a function of time, which could be applied to TCP Reno, and proved its equivalence to the previous, the well known TCP Reno model.

As the research on wireless networks becomes increasingly mature [14–16] and the application of TCP protocol is further expanded, we analyze the congestion fluid model for wireless networks and explore its dynamic behavior in the single-link case. The main contributions of this study are categorized into the following two aspects:

(1) With the τ-decomposition method for the linear analysis part proposed in this paper, we are able to quickly and accurately determine the equilibrium point of the system and its critical time delay using the modal equations, a process that is closely related to the static time delay feedback control. The method not only dramatically improves computational efficiency and accuracy, but also makes possible the analytic solution of the endpoints. In particular, the system exhibits Hopf bifurcation [17–21] at the endpoint when the time delay is used as the bifurcation parameter.

(2) In nonlinear part study of the system, we introduce the canonical type theory and the central manifold theorem [22–24] to explore the properties of the bifurcation solutions and reveal the direction of Hopf bifurcation and the stability of its periodic solutions. Different from the complex nonlinear methods (e.g., Lindstedt method [25]) commonly used in previous studies, our method greatly simplifies the algorithmic process, which not only improves the computational efficiency, but also makes the whole analytical process more concise and clearer.

Manuscript received: 21 November 2024; revised: 3 January 2025; accepted: 7 January 2025. *(Corresponding author: Tiaoyang Cai.)*

Citation: X. Yan, T. Cai, and R. Zhang, Stability and bifurcation of fluid flow model of TCP network versus time delay, *Int. J. Intell. Control Syst.*, 2025, 30(1), 38–46.

Xiaolu Yan and Tiaoyang Cai are with College of Engineering, Hebei Normal University, Shijiazhuang 050024, China (e-mail: yxl99127@outlook.com; chaoyang712@163.com).

Ranran Zhang is with Handan New District Power Supply Branch of State Grid Hebei Electric Power Co., Ltd., Handan 056000, China (e-mail: sgzrr0310@163.com).

Digital Object Identifier 10.62678/IJICS202503.10141

The rest of the paper is organized as follows. In Section II, we provide a preliminary analysis of the system and briefly introduce the τ-decomposition method. Section III is then divided into two main parts. First, in the linear analysis part, we analyze the characteristic equations related to the model by the τ-decomposition method and establish the existence conditions of the local Hopf bifurcation. Second, in the nonlinear analysis part, with the help of the central manifold theorem, we determine the direction of the Hopf bifurcation and the stability of the periodic solution. In Section IV, we provide several computational examples to verify the accuracy of the above theoretical results. Finally, in Section V, we summarize and discuss this study.

II. Local Stability and Existence of Hopf Bifurcation

A fluid flow model for TCP networks for congestion control in wireless networks was developed in Ref. [7], which also took into account packet loss due to transmission fading of the wireless channel. Its expression is

$$\begin{cases} \dot{W}(t) = \dfrac{1}{\tau(t)} - (1-P_{\mathrm{dl}})\dfrac{W(t)W(t-\tau(t))}{2\tau(t-\tau(t))}Q(t-\tau(t)) - \\ \qquad P_{\mathrm{dl}}(W(t)-1)\dfrac{W(t-\tau(t))}{\tau(t-\tau(t))}p(t-\tau_{\mathrm{ah}}(t)), \\ \dot{Q}(t) = N(1-P_{\mathrm{ul}})\dfrac{W(t)}{\tau(t)-C} \end{cases} \tag{1}$$

where t represents time. $W(t)$ denotes the size of the average TCP window. $Q(t)$ is the average queue length. $p(t)$ is the packet identification probability function. $N(t)$ is the number of TCP connections. C is the queue bandwidth. $\tau(t) = Q(t)/C(t) + T_p$ is the round-trip time consisting of transmission delay and queuing delay, where T_p represents the propagation delay of each stream and the subscript p is the packet identification probability function. $\tau_{\mathrm{ah}}(t)$ is the current time difference with the time when the latest identification probability is successfully received. When the queue delay is much smaller than the transmission delay, it can be assumed that $N(t) = N$ and $\tau_{\mathrm{ah}}(t) \approx \tau(t) = \tau$ are constants [5]. The probabilistic identity function is proportional to the queue length, yielding $p(t) = KQ(t)$, where K is a constant of proportionality, ignoring the window transmission delay. For wireless communication networks, some transmission packets may lose due to channel fading, P_{dl} and P_{ul} represent the downlink and uplink channel packet loss probabilities, respectively, and are assumed to be constants [5]. We simplify the above equation to

$$\begin{cases} \dot{W}(t) = \dfrac{1}{\tau} - \dfrac{(1+P_{\mathrm{dl}})W(t)^2 - 2P_{\mathrm{dl}}W(t)}{2\tau}KQ(t-\tau), \\ \dot{Q}(t) = N(1-P_{\mathrm{ul}})\dfrac{N}{\tau}W(t) - C \end{cases} \tag{2}$$

In this section, we first explore the local stability problem by considering the linear part of Eq. (2), where the unique equilibrium point (W_0, Q_0) is

$$W_0 = \frac{\tau C}{N(1-P_{\mathrm{ul}})},$$
$$p_0 = \frac{2}{(1+P_{\mathrm{dl}})W_0^2 - 2P_{\mathrm{dl}}W_0} = KQ_0.$$

Substituting two new variables $y_1(t) = W(t) - W_0$ and $y_2(t) = Q(t) - Q_0$ into the original Eq. (2) and linearizing it at the equilibrium point, we get

$$\begin{cases} \dot{y_1}(t) = \left[-\dfrac{1}{\tau}(1+P_{\mathrm{dl}})W_0p_0 + \dfrac{P_{\mathrm{dl}}}{\tau}p_0\right]y_1(t) + \\ \qquad \left[-\dfrac{1}{2\tau}(1+P_{\mathrm{dl}})W_0^2 + \dfrac{P_{\mathrm{dl}}}{\tau}W_0\right]Ky_2(t-\tau), \\ \dot{y_2}(t) = \dfrac{N}{\tau}(1-P_{\mathrm{ul}})y_1(t) \end{cases} \tag{3}$$

Obviously, Eq. (3) is modeled on Eq. (2) with the equilibrium point as the origin. We can rewrite the linear part of Eq. (3) in a matrix form as

$$\dot{u} = Au(t) + Bu(t-\tau) \tag{4}$$

with

$$A = \begin{bmatrix} -\dfrac{1}{\tau}(1+P_{\mathrm{dl}})W_0p_0 + \dfrac{P_{\mathrm{dl}}}{\tau}p_0 & 0 \\ \dfrac{N}{\tau}(1-P_{\mathrm{ul}}) & 0 \end{bmatrix},$$

$$B = \begin{bmatrix} 0 & \left[-\dfrac{1}{2\tau}(1+P_{\mathrm{dl}})W_0^2 + \dfrac{P_{\mathrm{dl}}}{\tau}W_0\right]K \\ 0 & 0 \end{bmatrix},$$

$$u(t) = \begin{bmatrix} y_1(t) \\ y_2(t) \end{bmatrix}.$$

From this we obtain the characteristic equation corresponding to Eq. (4) as

$$\begin{aligned} P(\lambda,\tau) = \det(\lambda I - A - B\mathrm{e}^{-\tau\lambda}) = \\ \lambda^2 + \left[\frac{1}{\tau}(1+P_{\mathrm{dl}})W_0p_0 - \frac{P_{\mathrm{dl}}}{\tau}p_0\right]\lambda - \\ \frac{N}{\tau}(1-P_{\mathrm{ul}})K\left[-\frac{1}{2\tau}(1+P_{\mathrm{dl}})W_0^2 + \right. \\ \left.\frac{P_{\mathrm{dl}}}{\tau}W_0\right]\mathrm{e}^{-\tau\lambda} \end{aligned} \tag{5}$$

where I stands for unit matrix and λ represents the eigenvalue.

Defining that

$$a_1 = \frac{1}{\tau}(1+P_{\mathrm{dl}})W_0p_0 - \frac{P_{\mathrm{dl}}}{\tau}p_0,$$
$$a_2 = -\frac{N}{\tau}(1-P_{\mathrm{ul}})K\left[-\frac{1}{2\tau}(1+P_{\mathrm{dl}})W_0^2 + \frac{P_{\mathrm{dl}}}{\tau}W_0\right],$$

then Eq. (4) becomes

$$\lambda^2 + a_1\lambda + a_2\mathrm{e}^{-\tau\lambda} = 0 \tag{6}$$

In order to ensure the stability of the above linear system, a necessary and sufficient condition must be satisfied: all eigenvalues lie in the left half-plane of the complex plane, which at the same time defines the stability interval of the time delay system (TDS). The τ-decomposition strategy is commonly used as an effective method for defining this stabilization region.

The τ-decomposition strategy covers two key task, computing pure imaginary roots (PIRs) and determining the direction in which these roots cross the imaginary axis. When dealing with the first task, given the symmetric nature of the conjugate complex roots about the real axis, we only need to focus on finding pure imaginary roots with positive values.

Introduce λ to denote the expressions A and C for the characteristic polynomial

$$P(\lambda) = A(\lambda) + C(\lambda)\mathrm{e}^{-\tau\lambda} = 0.$$

Let $\lambda = \pm j\omega$, then we have

$$\begin{cases} A(j\omega) + C(j\omega)\mathrm{e}^{-\tau j\omega} = 0, \\ A(-j\omega) + C(-j\omega)\mathrm{e}^{\tau j\omega} = 0. \end{cases}$$

This leads to the expression $\mathrm{e}^{\tau j\omega}$

$$\mathrm{e}^{\tau j\omega} = -\frac{C(-j\omega)}{A(-j\omega)}.$$

Therefore, we have

$$|A(j\omega)|^2 = |C(j\omega)|^2.$$

This shows that the two modal values are identical.

The second part of task determines the stability of the endpoint intersections, which depends on the direction of traversal on each pure imaginary root. The positive roots $\omega_1, \omega_2, \ldots, \omega_p$ are assumed to be unique and ordered from the largest to the smallest as $\omega_1 > \omega_2 > \cdots > \omega_p > 0$. Therefore, the largest root ω_1 is always traversed to the right, ω_2 is always traversed to the left, and so on. If there is only one positive root ω_1, all directions are to the right. If there are two positive roots, ω_1 is to the right and ω_2 is to the left.

Lemma 1 The transcendental Eq. (6) has only one pure imaginary root and

$$\omega_0 = \left[\frac{\sqrt{{a_1}^4 + 4{a_2}^2} - a_1^2}{2}\right]^{\frac{1}{2}} \tag{7}$$

with

$$a_1 = \frac{1}{\tau}(1 + P_{\mathrm{dl}})W_0 p_0 - \frac{P_{\mathrm{dl}}}{\tau}p_0,$$
$$a_2 = -\frac{N}{\tau}(1 - P_{\mathrm{ul}})K\left[-\frac{1}{2\tau}(1 + P_{\mathrm{dl}})W_0^2 + \frac{P_{\mathrm{dl}}}{\tau}W_0\right].$$

Proof 1 Proof of Lemma 1 Based on the above analysis, we can derive a characteristic equation for the system $P(\lambda, \tau)$. This equation is obtained by introducing the characteristic polynomials, denoted by A and C, associated with τ through the λ-decomposition strategy.

$$A(\lambda) = \lambda^2 + a_1\lambda,$$
$$C(\lambda) = a_2.$$

Considering the positive pure imaginary roots and setting $\lambda = j\omega_0$, we get

$$A(j\omega_0) = -{\omega_0}^2 + a_1 j\omega_0,$$
$$C(j\omega_0) = a_2.$$

From the equality of modulus values, it follows that

$${\omega_0}^4 + {a_1}^2{\omega_0}^2 - {a_2}^2 = 0.$$

Then, we have

$$\omega_0 = \left[\frac{\sqrt{{a_1}^4 + 4{a_2}^2} - a_1^2}{2}\right]^{\frac{1}{2}},$$

and obtain the result from Eq. (7). ■

Remark 1 Lemma 1 tells us that the TCP network fluid model has only one pure imaginary root, so it corresponds to a critical delay with uncertain traversal direction. Thus, according to the Laws criterion, we only need to consider the stability of the system at $\tau = 0$, i.e., $a_1 > 0$ and $a_2 > 0$.

In the previous discussion of the τ-decomposition method, we established that the traversal direction in the neighborhood of $j\omega_0$ is always to the right. Therefore, when we perform a local stability analysis of the linearized system in Eq. (3), the situation is described as follows.

Theorem 1 The equilibrium point (w_0, p_0) of Eq. (2) is exponentially stable when $\tau \in [0, \tau_0)$ and becomes unstable when $\tau \in (\tau_0, +\infty)$. And τ_0 is a Hopf bifurcation point.

$$\tau_0 = \arctan\left(\frac{a_1}{\omega_0}\right) \tag{8}$$

Proof 2 Proof of Theorem 1 By Lemma 1, only one set of equations in the characteristic polynomial has roots of $j\omega_0$. Based on the characteristic equations, we can conclude that

$$-{\omega_0}^2 + j\omega_0 a_1 + a_2\mathrm{e}^{-j\omega_0\tau_0} = 0.$$

Then, we obtain

$$\mathrm{e}^{j\omega_0\tau_0} = \frac{a_2}{-{\omega_0}^2 + j\omega_0 a_1}.$$

From this, the following result is obtained

$$\tau_0 = \arctan\left(\frac{a_1}{\omega_0}\right).$$

Finally, we obtain the result of Eq. (8). ■

Remark 2 Since ω_0 is an explicit expression for a_1 and a_2, τ_0 is also an explicit expression for a_1 and a_2. The simulation of τ_0 with respect to a_1 and a_2 is plotted in Fig. 1.

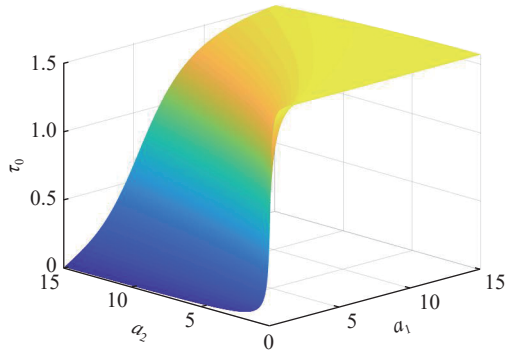

Figure 1 Simulation of τ_0 with respect to a_1 and a_2.

Based on the above analysis, the Hopf bifurcation exists as follows.

Remark 3 When $\tau < \tau_0$, Eq. (2) is locally stable, and all roots of the characteristic Eq. (6) are negative in real part. When $\tau > \tau_0$, Eq. (2) is unstable, and at least one of the roots

of the characteristic Eq. (6) is strictly positive in real part. If $\tau = \tau_0$, the roots of the characteristic Eq. (6) have negative real parts, at which point the system undergoes a Hopf bifurcation.

III. Directionality and Stability of Bifurcation Cycle Solution

The central manifold theorem and canonical type theory have a wide range of applications in dynamical system analysis. In this section, we combine these two theories to explore the direction of Hopf bifurcation and the stability of the periodic solutions generated by the bifurcation in the TCP network fluid model for congestion control in wireless networks.

First, we analyze the higher order terms of Eq. (2), which lead to the Taylor expansion of Eq. (2) at the equilibrium point, as shown in Eq. (9).

$$\begin{cases} \dot{y}_1(t) = a_{11}y_1(t) + a_{12}y_2(t-\tau) + a_{13}y_1^2(t) + \\ \quad a_{14}y_1(t)y_2(t-\tau) + a_{15}y_1^2(t)y_2(t-\tau), \\ \dot{y}_2(t) = a_{21}y_1(t) \end{cases} \tag{9}$$

The coefficients of the Taylor expansion are

$$\begin{aligned} a_{11} &= -\frac{1}{\tau}(1+P_{\mathrm{dl}})W_0 p_0, \\ a_{12} &= -\frac{1}{2\tau}(1+P_{\mathrm{dl}})W_0^2 + \frac{P_{\mathrm{dl}}}{\tau}W_0, \\ a_{13} &= -\frac{1}{\tau}(1+P_{\mathrm{dl}})p_0, \\ a_{14} &= -\frac{1}{\tau}(1+P_{\mathrm{dl}})W_0\frac{P_{\mathrm{dl}}}{\tau}, \\ a_{15} &= -\frac{1}{\tau}(1+P_{\mathrm{dl}}), \\ a_{21} &= \frac{N}{\tau}(1-P_{\mathrm{ul}}). \end{aligned}$$

We can reformulate the Taylor expansion in Eq. (9) into matrix form

$$\dot{y}(t) = Ay(t) + By(t-\tau) + F(y(t), y(t-\tau)) \tag{10}$$

with

$$F = \begin{bmatrix} f_1 \\ 0 \end{bmatrix},$$

and

$$f_1 = a_{13}y_1^2(t) + a_{14}y_1(t)y_2(t-\tau) + a_{15}y_1^2(t)y_2(t-\tau).$$

For the application of the Hopf bifurcation theorem, we need to convert Eq. (10) into an abstract system of differential equations and introduce $y_t(\theta)$ with time-delayed variable θ

$$y_t(\theta) = y(t+\theta) = \begin{bmatrix} y_1(t+\theta) \\ y_2(t+\theta) \end{bmatrix} \tag{11}$$

Differential operator L can be constructed with the linear part as a boundary condition

$$Lq(\theta) = \begin{cases} \dfrac{\mathrm{d}q}{\mathrm{d}\theta}, & -\tau \leqslant \theta < 0; \\ \displaystyle\int_{-\tau}^{0} q(\theta)\,\mathrm{d}\eta(\theta), & \theta = 0 \end{cases} \tag{12}$$

with eigenvector q and

$$\mathrm{d}\eta(\theta) = [A\delta(\theta) + B\delta(\theta+\tau)]\,\mathrm{d}\theta,$$

where $\delta(\cdot)$ represents the Dirac delta function.

Thereby, the functional differential equation can be reformulated as

$$\dot{y}_t(\theta) = Ly_t(\theta) + F(y_t) \tag{13}$$

with

$$F(y_t) = \begin{cases} 0, & -\tau \leqslant \theta < 0; \\ f(y_t), & \theta = 0, \end{cases}$$

where $f(\cdot)$ is a nonlinear function.

Next, in order to isolate the central manifold corresponding to $j\omega_0$, conjugate eigenvectors need to be computed to complete the projection.

We construct the inner product, bilinear form

$$\begin{aligned} \langle y^*, x\rangle &= \bar{y}^*(0)^{\mathrm{T}}x(0) + \int_{-\tau}^{0}\bar{y}^*(\xi+\tau)^{\mathrm{T}}Bx(\xi)\,\mathrm{d}\xi = \\ &\bar{y}^*(0)^{\mathrm{T}}x(0) + \tau\mathrm{e}^{-j\omega_0\tau_0}Bx(0) = \\ &\bar{y}^*(0)^{\mathrm{T}}[I + \tau_0\mathrm{e}^{-j\omega_0\tau_0}B]x(0) \end{aligned} \tag{14}$$

where $x \in [-\tau, 0]$ is a vector-valued continuous function and ξ is an integral variable.

Further, the conjugate operator L^* accompanying L can be induced which satisfies

$$L^*q^*(\theta) = \begin{cases} -\dfrac{\mathrm{d}q^*}{\mathrm{d}\theta}, & 0 < \theta \leqslant \tau; \\ \displaystyle\int_{-\tau}^{0}\mathrm{d}\eta(-\theta)^{\mathrm{T}}q^*(-\theta), & \theta = 0 \end{cases} \tag{15}$$

with

$$\mathrm{d}\eta(\theta)^{\mathrm{T}} = [A^{\mathrm{T}}\delta(\theta) + B^{\mathrm{T}}\delta(\theta+\tau)]\mathrm{d}\theta.$$

According to the theory of eigen-decomposition, what we need to compute is $q(\theta)$, the eigenvector of the linear operator L corresponding to $j\omega_0$. For this purpose, we state Lemma 2.

Lemma 2 In Eq. (12), $q(\theta)$ is represented as an eigenvector of L and is related to $j\omega_0$

$$q(\theta) = \begin{bmatrix} 1 \\ q_2 \end{bmatrix}\mathrm{e}^{j\omega_0\theta} \tag{16}$$

where

$$q_2 = \frac{a_{21}}{j\omega_0}.$$

Proof 3 Proof of Lemma 2 In Eq. (12), when θ lies in the range $[-\tau, \theta)$, the operation of the linear operator L can be understood simply as a derivation.

Moreover, considering the linear portion of the previously analyzed system, the differential operator corresponds to an eigenvalue of $\pm j\omega_0$. We denote by $j\omega_0$ the eigenvector of L associated with it, leading to the following relationship

$$q(\theta) = q(0)\mathrm{e}^{j\omega_0\theta}.$$

When $\theta = 0$, the action of the linear operator L is equivalent to performing the differentiation

$$Lq(0) = \int_{-\tau}^{0} q(\theta)\mathrm{d}\eta(\theta),$$

from that

$$Lq(\theta) = j\omega_0 q(\theta) = j\omega_0 q(0)\mathrm{e}^{j\omega_0\theta}.$$

The corresponding matrix form is

$$Aq(0) + Bq(0)\mathrm{e}^{-j\omega_0\tau_0} = j\omega_0 q(0),$$

and

$$\begin{cases} a_{11}q_1 + a_{12}q_2\mathrm{e}^{-j\omega_0\tau_0} = j\omega_0 q_1, \\ a_{21}q_1 = j\omega_0 q_2. \end{cases}$$

Let $q_1 = 1$, then $q_2 = a_{21}/(j\omega_0)$.

$$q(\theta) = q(0)\mathrm{e}^{j\omega_0\theta} = \begin{bmatrix} 1 \\ q_2 \end{bmatrix}\mathrm{e}^{j\omega_0\theta},$$

$$q_2 = \frac{a_{21}}{j\omega_0}.$$

From this, we can obtain Eq. (16). ■

Furthermore, for the conjugate eigenvectors, similar to previous discussion, Lemma 3 is made.

Lemma 3 In Eq. (15), $q^*(\theta)$ is an eigenvector of L^* and is associated with $-j\omega_0$

$$q^*(\theta) = D\begin{bmatrix} q_1^* \\ 1 \end{bmatrix}\mathrm{e}^{-j\omega_0\theta} \tag{17}$$

where

$$q_1^* = -\frac{a_{21}}{a_{11} + j\omega_0},$$

$$D = \frac{1}{\overline{\langle q, q_0^* \rangle}} = \frac{1}{q_{01}^* + \bar{q}_2(1 + q_{01}^* a_{21}\tau_0\mathrm{e}^{j\omega_0\tau_0})},$$

where q_0^* represents q^* with $\theta = 0$ and q_{01}^* is the first term of q_0^*.

Proof 4 Proof of Lemma 3 In Eq. (15), when θ lies in $(0, \tau]$, the operation of the conjugate linear operator L can be understood as finding the opposite of the derivative. We denote by $-j\omega_0$ the eigenvector of L^* associated with it, leading to the following relationship

$$q_0^*(\theta) = q_0^*(0)\mathrm{e}^{-j\omega_0\theta}.$$

When $\theta = 0$, the effect of the conjugate linear operator L^* is equivalent to differentiation, as described below

$$L^* q_0^*(\theta) = -j\omega_0 q_0^*(\theta) = -j\omega_0 q_0^*(0)\mathrm{e}^{j\omega_0\theta}.$$

Its corresponding matrix form is

$$A^{\mathrm{T}} q_0^*(0) + B^{\mathrm{T}} q_0^*(0)\mathrm{e}^{j\omega_0\tau_0} = -j\omega_0 q_0^*(0).$$

Then, we have

$$\begin{cases} a_{11}q_{01}^* + a_{21}q_{02}^* = -j\omega_0 q_{01}^*, \\ a_{12}q_{01}^*\mathrm{e}^{j\omega_0\tau_0} = -j\omega_0 q_{02}^*. \end{cases}$$

Let $q_{02}^* = 1$, then $q_{01}^* = -a_{21}/(a_{11} + j\omega_0)$.

$$q_0^*(\theta) = q_0^*(0)\mathrm{e}^{-j\omega_0\theta} = \begin{bmatrix} q_{01}^* \\ 1 \end{bmatrix}\mathrm{e}^{-j\omega_0\theta}.$$

However, in this case, $q_0^*(\theta)$ does not constitute a standard orthogonal basis. Therefore, to build the manifold within the coordinate system, we need to perform the necessary normalization using the inner product according to Eq. (14). The normalized eigenvector $q(\theta) = Dq_0^*(\theta)$ needs to satisfy $\langle q^*, Dq_0^* \rangle = 1$. Thus, we have

$$\langle q, q_0^* \rangle = \overline{q}_0^*(0)^{\mathrm{T}} q(0) + \mathrm{e}^{j\omega_0}\overline{q}_0^*(0)^{\mathrm{T}} Bq(0) = \frac{1}{\overline{D}},$$

and

$$D = \frac{1}{\overline{\langle q, q_0^* \rangle}} = \frac{1}{q_{01}^* + \bar{q}_2(1 + q_{01}^* a_{21}\tau_0\mathrm{e}^{j\omega_0\tau_0})}.$$

This leads to Eq. (17). ■

In the above procedure, we detail the solution of the operator and its accompanying forms and equations, which lead to $q(\theta)$ and $q^*(\theta)$. From this, we are able to identify the accompanying vectors and distinguish the solution space as central manifolds and stable manifolds.

$$\begin{cases} z(t) = \langle q^*, y_t \rangle, \\ w(t,\theta) = y_t(\theta) - z(t)q(\theta) - \bar{z}(t)\bar{q}(\theta) \end{cases} \tag{18}$$

where $z(t)$ is the center manifold representing the projection of solution manifold $y_t(\theta)$ along the direction of adjoint vector $q^*(\theta)$. $w(t)$ corresponds to the stable manifold, and the sum of $w(t)$ and $z(t)$ constitutes $y_t(\theta)$.

Lemma 4 The evolution of z with time t can be expressed as

$$\dot{z}(t) = j\omega_0 z + \frac{1}{2}g_{20}z^2 + g_{11}z\bar{z} + \frac{1}{2}g_{02}\bar{z}^2 + \frac{1}{2}g_{21}(\theta)z^2\bar{z} + \cdots \tag{19}$$

and

$$\begin{aligned} g_{20} &= \overline{q}_1^* f_{201}, \\ g_{11} &= \overline{q}_1^* f_{111}, \\ g_{02} &= \overline{q}_1^* f_{021}, \\ g_{21} &= \overline{q}_1^* f_{211} \end{aligned} \tag{20}$$

where f has the following specific tabular forms

$$\begin{aligned} f_{201} &= a_{13} + a_{14}q^{(2)}(-\tau_0), \\ f_{111} &= 2a_{13} + a_{14}[q^{(2)}(-\tau_0)\bar{q}^{(2)}(-\tau_0)], \\ f_{021} &= a_{13} + a_{14}\bar{q}^{(2)}(-\tau_0), \\ f_{211} &= a_{13}[2W_{11}^{(1)}(0) + W_{20}^{(1)}(0)] + a_{14}[W_{11}^{(2)}(-\tau_0) + \\ &\quad \frac{1}{2}W_{20}^{(2)}(-\tau_0) + \frac{1}{2}W_{20}^{(1)}(0)q^{(2)}(-\tau_0) + \\ &\quad W_{11}^{(1)}(0)q^{(2)}(-\tau_0)] + a_{15}[\bar{q}^{(2)}(-\tau_0) + 2q^{(2)}(-\tau_0)] \end{aligned} \tag{21}$$

where the subscript $(\cdot)$ indicates the $(\cdot)$-th term of the variable. W_{11} and W_{20} correspond to the coefficient functions of z^2 and $z\bar{z}$, respectively, when the stable state $w(t,\theta)$ is expanded according to the canonical type.

Proof 5 Proof of Lemma 4 Near the origin O, with q and $\bar{q}$ as the local coordinate directions, $z(t)$ and $\bar{z}(t)$ are the

manifolds in C. According to Eqs. (18) and (19), the evolution of the central manifolds can be derived as

$$\begin{aligned}\dot{z}(t) &= \langle q^*, \dot{y}_t\rangle = \langle q^*, Ly_t(0) + Fy_t(0)\rangle = \\ &\langle q^*, Ly_t(0)\rangle + \langle q^*, Fy_t(0)\rangle = \\ &j\omega_0 z(t) + \bar{q}^*(0)^{\mathrm{T}} Fy_t(0) = \\ &j\omega_0 z + \bar{D}[1\ \bar{q}_2^*][F_{20}z^2 + F_{11}z\bar{z} + F_{02}\bar{z}^2 F_{21}z^2\bar{z} + \cdots],\end{aligned}$$

and

$$F_{20} = \begin{bmatrix} f_{201} \\ f_{202}\end{bmatrix},\ F_{11} = \begin{bmatrix} f_{111} \\ f_{112}\end{bmatrix},$$

$$F_{02} = \begin{bmatrix} f_{021} \\ f_{022}\end{bmatrix},\ F_{21} = \begin{bmatrix} f_{211} \\ f_{212}\end{bmatrix},$$

where $f_{202} = f_{112} = f_{022} = f_{212} = 0$ and the specific expressions for f_{201}, f_{111}, f_{021}, and f_{211} are shown in Eq. (21).

Based on the central manifold theorem, Eq. (18) shows that

$$w(t,\theta) = \frac{1}{2}W_{20}(\theta)z^2(t) + W_{11}(\theta)z(t)\bar{z}(t) + \cdots.$$

According to the theorem, it can be obtained that

$$y_t(\theta) = z(t)q(\theta) + \bar{z}(t)\bar{q}(\theta) + \frac{1}{2}y_{20}(\theta)z^2(t) + y_{11}(\theta)z(t)\bar{z}(t) + \cdots,$$

where y_{20} and y_{11} are coefficient functions.

Based on Eq. (11), we can obtain

$$y_t(\theta) = \begin{bmatrix} y_{1t}(\theta) \\ y_{2t}(\theta)\end{bmatrix} = \begin{bmatrix} y_1(t+\theta) \\ y_2(t+\theta)\end{bmatrix}.$$

The system is then converted to the form y

$$\begin{cases} y_1(t) = y_1(t+0) = y_t^{(1)}(0), \\ y_2(t) = y_2(t+0) = y_t^{(2)}(0), \\ y_1(t-\tau) = y_1(t+(-\tau)) = y_t^{(1)}(-\tau), \\ y_2(t-\tau) = y_2(t+(-\tau)) = y_t^{(2)}(-\tau). \end{cases}$$

We specify the y used, which gives us

$$\begin{aligned} y_t^{(1)}(0) &= zq^{(1)}(0) + \bar{z}\bar{q}^{(1)}(0) + \frac{1}{2}W_{20}^{(1)}(0)z^2 + W_{11}^{(1)}(0)z\bar{z}, \\ y_t^{(2)}(-\tau) &= zq^{(2)}(-\tau) + \bar{z}\bar{q}^{(2)}(-\tau) + \frac{1}{2}W_{20}^{(2)}(-\tau)z^2 + \\ &\quad W_{11}^{(2)}(-\tau)z\bar{z}. \end{aligned}$$

By introducing the nonlinear components of the system, we are able to obtain expressions in Eq. (21) for f_{201}, f_{111}, f_{021}, and f_{211}, which leads to

$$\begin{aligned} g_{20} &= \bar{q}_1^* f_{201}, \\ g_{11} &= \bar{q}_1^* f_{111}, \\ g_{02} &= \bar{q}_1^* f_{021}, \\ g_{21} &= \bar{q}_1^* f_{211}. \end{aligned}$$

It is easy to see that the system parameters can be directly determined for g_{20}, g_{11}, and g_{02}. Nevertheless, g_{21} is also related to W_{20} and W_{11}. ■

The calculation of $W_{20}(\theta)$ and $W_{11}(\theta)$ is described below.

Lemma 5 According to Ref. [22], W_{20} and W_{11} are coefficients of the center manifold $x(t)$ with following form

$$\begin{cases} W_{20}(\theta) = \dfrac{g_{20}j}{\omega_0}q(0)\mathrm{e}^{\theta j\omega_0} + \dfrac{\bar{g}_{02}j}{3\omega_0}\bar{q}(0)\mathrm{e}^{-\theta j\omega_0} + E_{20}\mathrm{e}^{2\theta j\omega_0}, \\ W_{11}(\theta) = -\dfrac{g_{11}j}{\omega_0}q(0)\mathrm{e}^{\theta j\omega_0} + \dfrac{\bar{g}_{11}j}{\omega_0}\bar{q}(0)\mathrm{e}^{-\theta j\omega_0} + E_{11} \end{cases} \tag{22}$$

with

$$\begin{cases} E_{20} = \begin{bmatrix} \dfrac{2j\omega_0 f_{201}}{4\omega_0^2 + 2a_{11}j\omega_0 + a_{12}a_{21}\mathrm{e}^{-2\omega_0\tau_0}} \\ \dfrac{a_{21}}{2j\omega_0}E_{20}^{(1)} \end{bmatrix}, \\ E_{11} = \begin{bmatrix} 0 \\ -\dfrac{f_{111}}{a_{12}} \end{bmatrix} \end{cases} \tag{23}$$

In summary, we obtained all expressions for g function

$$C_1(0) = \frac{j}{2\omega_0}\left(g_{20}g_{11} - 2|g_{11}|^2 - \frac{1}{3}|g_{02}|^2\right) + \frac{g_{21}}{2} \tag{24}$$

where C_1 is the Lyapunov coefficient.

Thus, we can generalize the following nonlinear dynamics theorem for Eq. (2)

$$\begin{cases} \mu_2 = -\dfrac{\mathrm{Re}\{C_1(0)\}}{\alpha'(0)}, \\ \beta_2 = 2\mathrm{Re}\{C_1(0)\}, \\ \tau_2 = -\dfrac{\mathrm{Im}\{C_1(0)\} + \mu_2\omega'(0)}{\omega_0} \end{cases} \tag{25}$$

where α' and ω' represent the real part and imaginary part of the eigenvalue, respectively.

Based on the canonical type theory and the central manifold theorem, we can conclude the Hopf bifurcation of Eq. (2). This approach allows us to determine specific values for all bifurcation parameters.

$$-\left.\frac{\dfrac{\partial P}{\partial \tau}}{\dfrac{\partial P}{\partial \lambda}}\right|_{(\tau_0,\ j\omega_0)} = \alpha'(0) + j\omega'(0).$$

Theorem 2 For Eq. (2), the direction of the Hopf bifurcation and the stability of its periodic solution are determined by Eq. (25) and the following parameters.

(1) The direction of the Hopf bifurcation is determined by $\mu_2 = -C_{1\mathrm{R}}(0)/\alpha'(0)$, if $\mu_2 > 0\ (< 0)$, the Hopf bifurcation is supercritical (subcritical) and the bifurcation periodic solution exists when $\tau > \tau_0\ (\tau < \tau_0)$.

(2) The stability of the Hopf bifurcation cycle solution is determined by $\beta_2 = 2C_{1\mathrm{R}}(0)$, if $\beta_2 < 0\ (> 0)$, the bifurcation cycle solution is stable (unstable).

(3) The period of the Hopf bifurcation period solution is determined by $\tau_2 = -(C_{1I}(0) + \mu_2\omega'(0))/\omega_0$, and the period is increasing (decreasing) if $\tau_2 > 0\ (< 0)$.

IV. Numerical Example

In this section, we present several typical simulations used to verify the accuracy of the obtained results. The calculations

are done with the help of Matlab and Mathematica. The analyzed results show that the method is able to effectively deal with the nonlinear dynamics of the TCP system.

We choose system parameters $N=50$, $K=0.001$, $C=1000$, and $P_{\mathrm{dl}}=P_{\mathrm{ul}}=0.1$.

$$\begin{cases}\dot{W}(t)=\dfrac{1}{\tau}-\dfrac{((1+0.1)W(t)^2-2\times 0.1W(t))}{2\tau}0.001\times Q(t-\tau),\\ \dot{Q}(t)=(1-0.1)\dfrac{50}{\tau}W(t)-1000.\end{cases}$$

Based on the characteristic Eq. (6), we can conclude that

$$\lambda^2+2.2986\lambda+11.7220\mathrm{e}^{-\lambda\tau}=0.$$

It follows from Lemma 1 that

$$\omega_0 = 3.0617.$$

Moreover, from Theorem 1 we obtain the critical time delay as

$$\tau_0=0.3131.$$

Based on the above results, we can conclude that the point (a_1,a_2,τ_0) is in the simulation plane, as shown in Fig. 2.

Through simulation experiments, we obtain the time delay stability range. Combined with the aforementioned theoretical calculations, it can be seen that the range derived from the theoretical analysis is consistent with the simulation results, thus mutually confirming the validity of both sides.

In the root trajectory diagram (see Fig. 3), when $\tau_0<0.3131$, all the characteristic roots have negative real parts, indicating that the system remains stable under this condition. In addition, when $\tau=0.3131$, there is a pair of purely imaginary roots crossing the imaginary axis, which triggers unstable oscillations, i.e., a Hopf bifurcation occurs in the system at this point. Therefore, for the TCP transmission system, the stable time delay interval is $[0,0.3131]$. This finding further confirms the high agreement between the theoretical analysis and the simulation results.

Calculating the relevant parameters based on Lemmas 2 and 3 produces the following accompanying vectors

$$q(\theta)=\begin{bmatrix}\mathrm{e}^{(0+3.0617j)\theta}\\(0-73.488585j)\mathrm{e}^{(0+3.0617j)\theta}\end{bmatrix},$$

$$q^*(\theta)=\begin{bmatrix}(0.000075+0.010650j)\mathrm{e}^{(0-3.0617j)\theta}\\(0.000146+0.000108j)\mathrm{e}^{(0-3.0617j)\theta}\end{bmatrix}.$$

Combining this with Lemma 4, we get

$$g_{20}=10.876934-15.256044j,$$
$$g_{11}=11.322165-14.606721j,$$
$$g_{02}=-10.661677-15.407246j.$$

Next, Lemma 5 describes W_{20} and W_{11}

$$W_{20}(-\tau)=\begin{bmatrix}-0.422185-5.703936j\\-59.559984-198.072149j\end{bmatrix},$$

$$W_{11}(-\tau)=\begin{bmatrix}-11.535952\\287.990116+20.219729j\end{bmatrix}.$$

Then, we have

$$g_{21}=-140.646297+162.834436j.$$

Thereby, the bifurcation parameters are given by Eq. (25)

$$\begin{cases}\beta_2=-114.399859,\\ \mu_2=11.1365131,\\ \tau_2=-210.6100.\end{cases}$$

Theorem 3 states that the system undergoes a Hopf bifurcation at $\tau_0=0.3131$ and the direction of the bifurcation is supercritical.

The simulation plots, Fig. 4 with $\tau=0.1800$ and Fig. 5 with $\tau=0.2000$, show that the trajectory converges to a point when $\tau<\tau_0$ and the system is stable.

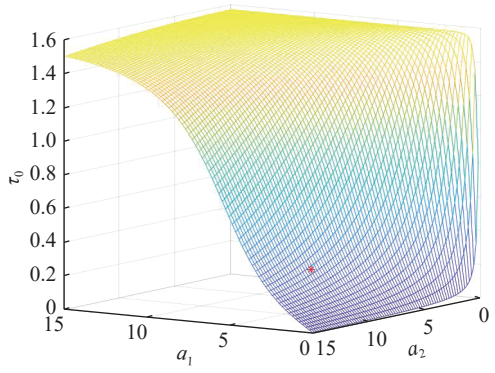

Figure 2 Bifurcation point in simulation plane.

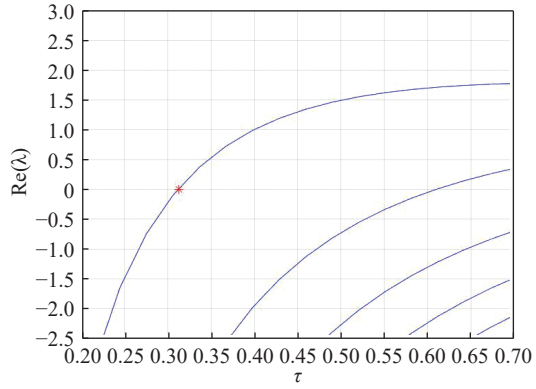

Figure 3 Rightmost root locus as a function of delay τ.

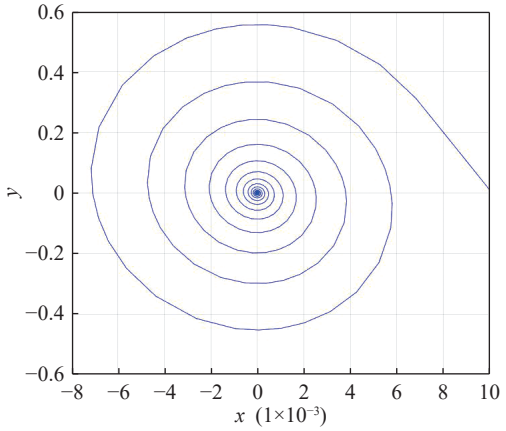

Figure 4 Stable phase trajectory exhibiting delay within a stable interval ($\tau=0.1800$).

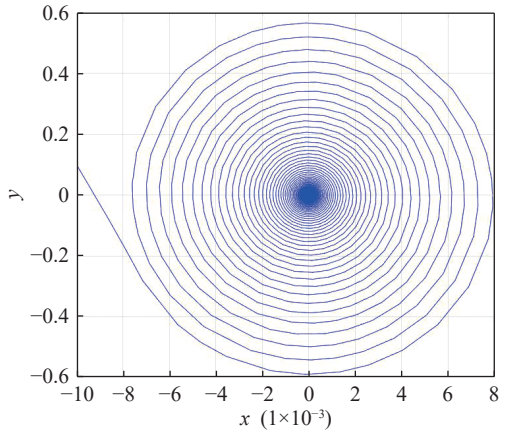

Figure 5 Stable phase trajectory exhibiting delay within a stable interval ($\tau = 0.2000$).

In the simulation plot, Fig. 6 with $\tau = 0.3131$, we take a particular bifurcation point $\tau_0 = 0.3131$. We find that as the time delay changes, the system no longer tends toward the equilibrium point. As shown in Theorem 1, $\tau_0 = 0.3131$ is the bifurcation point where the Hopf bifurcation occurs and the trajectory converges to the limit ring, i.e., there exists a phase trajectory with periodic convergence. It is calculated that β_2 is less than 0 and the periodic trajectory is stable. When $\tau_2 > 0$, the period of the periodic solution increases with τ.

Figure 7 illustrates the simulation curves at $\tau = 0.5540$, and comparing Fig. 6 and Fig. 7, it can be seen that the orbital period at $\tau = 0.5540$ is longer than that at $\tau_0 = 0.3131$.

V. Conclusion

In this study, we explore the TCP network fluid model. By employing a τ-decomposition strategy and using the nonlinear interaction strength as the bifurcation parameter, we determine the maximum value of the time delay stabilization boundary. The results show that when this parameter exceeds its critical value, the simplified model undergoes the Hopf bifurcation and the state of the system changes from an equilibrium point to a series of periodic solutions. Using the regular expression theory and the central manifold theorem, we analyze the nonlinear part and clarify the stability and direction of the bifurcation cycle solution. Experimental simulations confirm the correctness of the theoretical analysis.

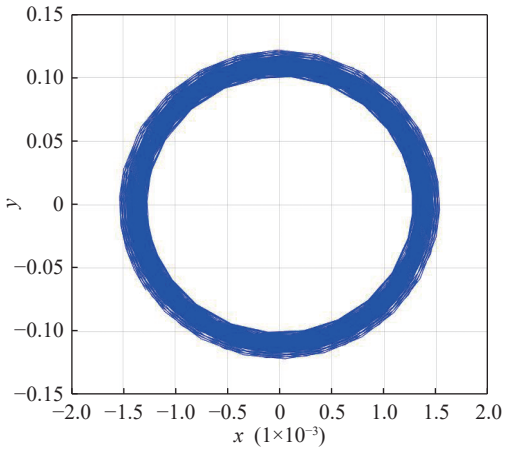

Figure 6 Bifurcated phase path with delay ($\tau_0 = 0.3131$).

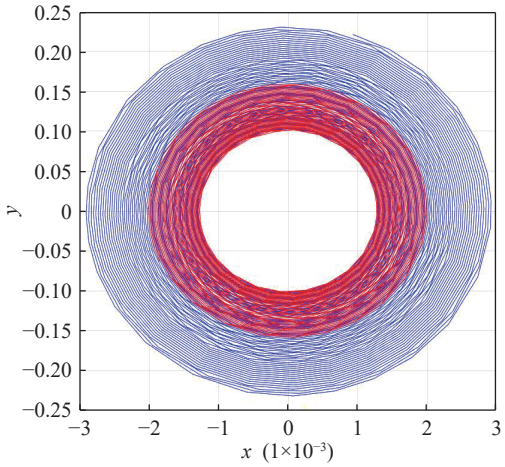

Figure 7 Two phase trajectories featuring delay within unstable interval ($\tau = 0.5540$).

References

[1] Q. Gao, J. Li, Y. Liu, and Y. Xing, Optimal control method for congestion control and delay reduction in deterministic networks, *IEEE Access*, 2023, 11, 82912–82923.

[2] P. Anitha, H. S. Vimala, and J. Shreyas, Comprehensive review on congestion detection, alleviation, and control for IoT networks, *J. Netw. Comput. Appl*., 2024, 221, 103749.

[3] G. Sun, C. Li, Y. Ma, S. Li, and J. Qiu, End-to-end TCP congestion control as a classification problem, *IEEE Trans. Reliab*., 2023, 72(1), 384–394.

[4] K. S. Midhula and P. A. R. Kumar, An adaptive congestion control protocol for wireless networks using deep reinforcement learning, *IEEE Trans. Netw. Serv. Manage*., 2024, 21(2), 2027–2043.

[5] F. Zheng and J. Nelson, An H_∞ approach to congestion control design for AQM routers supporting TCP flows in wireless access networks, *Comput. Netw*., 2007, 51(6), 1684–1704.

[6] J. Chen and Y. Jing, Multiple bottleneck topology TCP/AQM switching network congestion control with input saturation and prescribed performance, *ISA Trans*., 2023, 135, 369–379.

[7] J. Shen, Y. Jing, and G. M. Dimirovski, Fixed-time congestion tracking control for a class of uncertain TCP/AQM computer and communication networks. *Int. J. Control, Autom. Syst*., 2022, 20(3), 758–768.

[8] D. Ghosh, K. Jagannathan, and G. Raina, Local stability and Hopf bifurcation analysis for compound TCP, *IEEE Trans. Control Netw. Syst*., 2018, 5(4), 1668–1681.

[9] H.-L. Jin, T.-L. Di, H. Yu, and R.-R. Zhang, On the τ decomposition method for the stability and bifurcation of the TCP/AQM networks versus time delay, *Symmetry*, 2022, 14(3), 463.

[10] H. Yu, S. Guo, F. Wang, and Y. Yang, Dynamic time-delayed feedback control of Westwood+ TCP flow control model with communication delay, *IMA J. Math. Control Inf*., 2018, 35(3), 1005–1025.

[11] T. Cai, X. Yan, and R. Zhang, A reliable algorithm for the characterization of the nonlinear dynamics of FAST TCP networks, *IEEE Access*, 2024, 12, 40544–40554.

[12] S. Manjunath and G. Raina, Stability and performance of compound TCP with a proportional integral queue policy, *IEEE Trans. Control Syst. Technol*., 2019, 27(5), 2139–2155

[13] G. Vardoyan, C. V. Hollot, and D. Towsley, Towards stability analysis of data transport mechanisms: A fluid model and its applications, *IEEE ACM Trans. Netw*., 2021, 29(4), 1730–1744.

[14] H. Pirayesh and H. Zeng, Jamming attacks and anti-jamming strategies in wireless networks: A comprehensive survey, *IEEE Commun. Surv. Tutorials*, 2022, 24(2), 767–809

[15] S. He, An endogenous intelligent architecture for wireless communication networks, *Wirel. Netw*., 2024, 30(2), 1069–1084.

[16] M. B. Patil and R. Patil, Fuzzy based network controlled vertical handover mechanism for heterogeneous wireless network, *Mater. Today: Proc*., 2023, 80(Pt3), 2385–2389.

[17] Y. Song and Q. Shi, Stability and bifurcation analysis in a diffusive predator–prey model with delay and spatial average, *Math. Methods Appl. Sci*., 2023, 46(5), 5561–5584.

[18] S. Guo, Global Hopf bifurcation of state-dependent delay differential equations, *Int. J. Bifurcat. Chaos*, 2023, 33(6), 2350074.

[19] X. Chang, X. Gao, and J. Zhang, Hopf bifurcation analysis of a housefly model with time delay, *Int. J. Bifurcat. Chaos*, 2023, 33(9), 2350106.

[20] X. Wu, L. Wang, B. Bai, J. Qiao, and A. Fei, Hopf bifurcation in DCTCP congestion control, *IEEE Commun. Lett*., 2020, 24(7), 1424–1427.

[21] D. Liu and W. Jiang, Steady-state bifurcation and Hopf bifurcation in a reaction-diffusion-advection system with delay effect, *J. Dyn. Differ. Equ*., 2024, 36(2), 1777–1817.

[22] T.-Y. Cai, H.-L. Jin, H. Yu, and X.-P. Xie, On stability switches and bifurcation of the modified autonomous van der Pol-duffing equations via delayed state feedback control, *Symmetry*, 2021, 13, 2336.

[23] C. Kasnakoglu and A. Serrani, Analysis and nonlinear control of Galerkin models using averaging and center manifold theory, in *Proc. 2007 American Control Conference*, New York, NY, USA, 2007, 3035–3040.

[24] X. Ding and X. Zheng, Forms of entire solutions of partial differential difference equations with constant coefficients, *Electron. J. Differ. Equ*., 2024, 2024(37), 1–15.

[25] I. B. Tagne Nkounga, F. M. Moukam Kakmeni, and R. Yamapi, Birhythmic oscillations and global stability analysis of a conductance-based neuronal model under ion channel fluctuations, *Chaos, Solitons Fractals*, 2022, 159, 112126.

Xiaolu Yan received the BS degree in Internet of Things from Huihua College, Hebei Normal University, China, in 2022. She is currently pursuing the MS degree in software engineering at Hebei Normal University, China. Her research interests include network congestion control and nonlinear dynamics of time delay system.

Tiaoyang Cai received the BSc degree in computer science and technology from Hebei University of Engineering, China, in 2002, the MSc degree in control engineering from Hebei Polytechnic University, China, in 2009, and the PhD degree in control theory from Northeastern University, China, in 2014. He is currently an associate professor at College of Engineering, Hebei Normal University, China. His research interests include time delay systems, proportional-integral-derivative (PID) control, and nonlinear dynamic analysis of TDS.

Ranran Zhang received the BSc degree in electrical engineering and automation from Hebei Normal University, China, in 2016. She is currently an employee at Handan New District Power Supply Branch of State Grid Hebei Electric Power Co., Ltd., Handan, China. Her research interests include power systems, PID control, and nonlinear dynamics of time delay system.